PHYSICAL REVIEW D **91,** 101301(R) (2015)

# Probing the spacetime around supermassive black holes with ejected plasma blobs

Pierre Christian and Abraham Loeb

*Harvard Smithsonian Center for Astrophysics, 60 Garden Street, Cambridge, Massachusetts 02138, USA*

(Received 19 March 2015; published 8 May 2015)

Millimeter-wavelength very-long-baseline-interferometry observations of the supermassive black holes in Sgr A* and M87 by the Event Horizon Telescope could potentially trace the dynamics of ejected plasma blobs in real time. We demonstrate that the trajectory and tidal stretching of these blobs can be used to test general relativity and set new constraints on the mass and spin of these black holes.

DOI: 10.1103/PhysRevD.91.101301 PACS numbers: 97.60.Lf, 95.10.Ce, 97.10.Wn

## I. INTRODUCTION

The planned Event Horizon Telescope (EHT)[1] will possess angular resolution comparable to the Schwarzschild radius of the supermassive black holes, Sgr A* and the one at the center of M87, and temporal resolution on minute time scales [1]. This is expected to open a new avenue for studying a multitude of transient phenomena under extreme gravity.

Sgr A* is known to exhibit variability with a time scale of tens of minutes corresponding to accretion disk activity at the innermost stable circular orbit (ISCO) [1,2]. Here we study a hypothetical class of short time-scale events corresponding to plasma blobs ejected near the ISCO radius. Although such blobs were never observed from a supermassive black hole, they may exist based on the analogy with microquasars, which are known to propel blobs at relativistic speeds [3–5].

In addition to microquasars, plasma blob ejection is also observed in the Sun during coronal mass ejection (CME) events [6,7]. Microquasars and stars have very different magnetic field and gas properties, and the presence of blob ejections in both of them leads us to believe that plasma blob ejections are a generic phenomenon in magnetized environments. In particular, it has been suggested that plasma ejections for both microquasars and CMEs are caused by magnetic reconnection [6,8], and in the past CME has been argued to be analogous to blob launching in microquasars [9]. Since magnetic reconnection is likely operating in the turbulent accretion disk around both Sgr A* and M87, plasma blob ejections can be expected to occur in these environments.

The second target of the EHT is the supermassive black hole at the center of the elliptical galaxy M87. In contrast to Sgr A*, M87 possesses a jet, and it is likely that blobs are ejected along the jet's symmetry axis.

In this paper, we demonstrate that if ejected plasma blobs are detected, one could use their dynamics to probe the spacetime around the black holes. Furthermore, if the mass and spin of a given black hole are known, one can use observations of the blob's dynamics to test general relativity or infer the presence of nongravitational sources such as gas pressure or magnetic stress. These constraints would be complementary to constraints from pulsar timing [10–14] or observations of the black hole shadow [15–17].

There are two elements of dynamical information: the trajectory of the blob's center of mass and its lateral expansion. Both can be used to independently constrain the black hole's spacetime. We discuss the former in Secs. II and III, and the later in Sec. IV. Throughout the discussion, we will assume general relativity. Deviations from our results would indicate the presence of nongravitational forces or corrections to the theory of gravity. We use units where $G = c = 1$, and the conversion from these units to physical units is given in Table I.

## II. CENTER-OF-MASS MOTION

First we consider the motion of the blob's center of mass (COM). If the blob is ejected above the escape speed from the ISCO radius, $R_{\rm ISCO}$, its azimuthal velocity will be negligibly small at $r \gg R_{\rm ISCO}$, so we focus our discussion on the radial equation of motion. For a Schwarzschild black hole [23],

$$\left(\frac{dy}{d\tau}\right)^2 = \frac{2M}{r} - (1-e^2); \qquad \frac{dt}{d\tau} = \frac{e}{1-2M/r}, \quad (1)$$

where $M$ is the black hole mass, $e$ the energy per unit rest mass of the blob, $r$ the black hole-blob distance, $t$ the coordinate time, and $\tau$ the blob's proper time. These two equations can be solved for $dt/dr$ and integrated to obtain the coordinate time as a function of the orbital radius of the blob's COM,

$$t_{\rm Sch}(r) = \int_{R_{\rm ISCO}}^{r} \frac{e}{(1-\frac{2M}{r'})\sqrt{\frac{2M}{r'}-(1-e^2)}}\,dr'. \quad (2)$$

If the blob is ejected out of a Kerr black hole, a similar set of equations can be solved to obtain its COM motion in the equatorial plane,

[1]See http://www.eventhorizontelescope.org.

 

TABLE I. The conversion of black hole mass $M$ to units of time, space, and angular size on the sky for Sgr A* and M87 [18–22], for $G = c = 1$.

| | Black hole mass | Distance | Time | Space | Angle |
|---|---|---|---|---|---|
| Sgr A* | $(4.31 \pm 0.36) \times 10^6 M_\odot$ | $7.94 \pm 0.42$ kpc | 21 s | 0.043 AU | 5.3 $\mu$as |
| M87 | $(3.5^{+0.9}_{-0.7}) \times 10^9 M_\odot$ | $16.7 \pm 0.9$ Mpc | 4.8 hr | 35 AU | 2.1 $\mu$as |

$$t_{\rm Kerr}(r) = \int_{R_{\rm ISCO}}^{r} \frac{e}{\Delta} \frac{r'^2 + a^2 + \frac{2a^2M}{r'}}{\sqrt{e^2 + \frac{2Ma^2e^2}{r'^3} + \frac{a^2e^2}{r'^2} - \frac{\Delta}{r'^2}}} dr', \quad (3)$$

where $a$ is the black hole's spin parameter and $\Delta(r) \equiv r^2 - 2Mr + a^2$. In general, there is no reason for the blob to be ejected in the equatorial plane of the black hole, and in fact blobs should preferentially be ejected along the spin axis. But, as shown in Fig. 1, the effect of the black hole spin is weak. At $t = 10M$, the trajectory of a blob with $e = 2$ launched from an $a = 0.999$ black hole is only $0.36M$ apart from one launched from an $a = 0$ black hole.

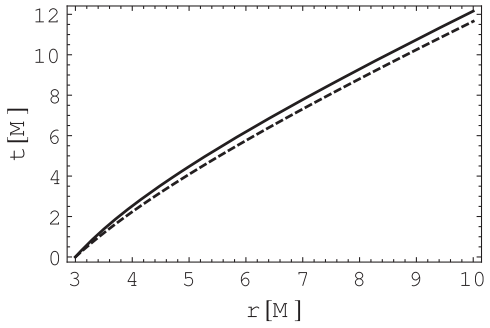


FIG. 1. The radial motion of blobs with $e = 2$ in the equatorial plane of a black hole with $a = 0$ (solid line) and $a = 0.999$ (dotted line).

## III. RAY TRACING

In simulating what would be seen by radio interferometers, we project the COM motion of the blob to the sky plane far from the black hole. We utilize the *geokerr* code [24] to trace rays from the observer plane located at infinity to the position of the blob. The coordinates $(x, y)$ parametrize positions in this observer plane. The Fourier transform of this plane yields the visibility of a radio interferometer.

The blob itself is modeled as a small sphere that is emitting isotropically in its rest frame. The result for blobs with velocity vectors at angles $\theta = 0$ and $\theta = \pi/8$ away from the observer are presented in Fig. 2. For a blob moving along the $\theta = 0$ axis, the image is briefly lensed into a ring with radius $R_{\rm ring} \sim 5M$. Previous calculations by [25] showed that the eccentricity of this ring is not sensitive to the spin of the black hole (except for $a \approx 1$), but it is very sensitive to the black hole's quadrupole moment. Thus, if detected, the ring can be used as a test of the no-hair theorem. As the ring only appears when the blob is still close to the black hole, its lifetime is short ($\sim 40M$ for a blob with $e = 10$, but longer for slower moving blobs). It is therefore necessary to have temporal resolutions on a minute time scale to detect the ring.

In addition, if the motion is fast enough and is launched at a small angle relative to the observer, the apparent trajectory can appear superluminal (e.g., Ref. [26]). Close to the black hole, this apparent superluminal motion will be obscured by the bright photon ring. Thus, the detection of superluminal motion will require either waiting for the ring to dim or a manual removal of the ring.

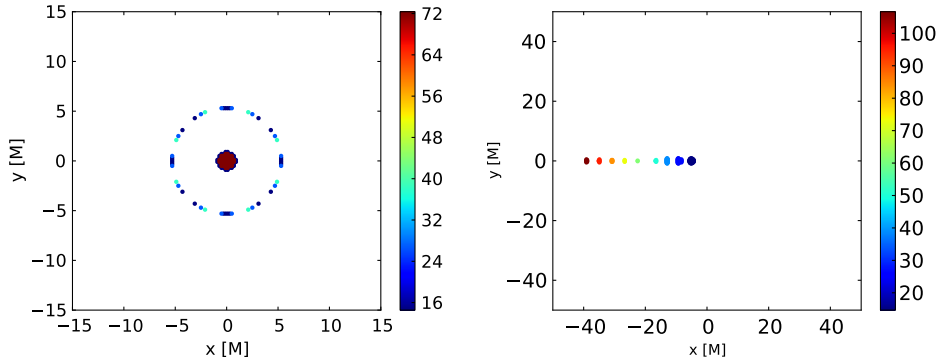


FIG. 2 (color online). Blobs with $e = 10$ and radius $M$ launched with $\theta = 0$ and $\theta = \pi/8$ as seen in the observer plane with the black hole located at (0,0). The observer's time axis (in units of $M$) is indicated by the color bar. For a blob moving with $\theta = 0$, the image is briefly lensed into a ring. The eccentricity of this ring can be used to test the no-hair theorem.

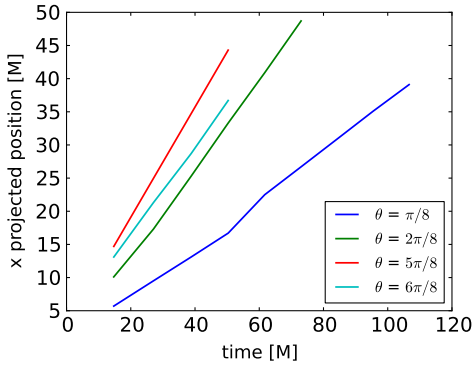


FIG. 3 (color online). The projected position of blobs with $e = 10$ launched at a variety of angles versus observer time.

The projected distance as a function of observed times, shown in Fig. 3, can be compared with observations to determine the presence of nongravitational forces (e.g., due to magnetic fields or hydrodynamic friction on background gas). In addition, it can be used to constrain gravitational theories that predict changes on the orbit of test particles close to a black hole (e.g., Ref. [27]).

## IV. TIDAL EFFECTS

If the forces holding the blob together are much smaller than the tidal gravitational forces, the blob will be tidally sheared. The magnitude of this tidal shear depends on the black hole's mass and spin and thus can be used to probe the black hole metric. Under the approximation that the force per unit mass keeping the blob together is $\ll(2MR/r^3)$, where $R$ is the radius of the blob, the elements of the blob can be treated as if they are moving along geodesics.

If the blob is small, we can define the geodesic deviation vector $\xi^\alpha$ between the geodesic followed by the particle at the center of the blob and the different geodesic followed by particles at the blob's edge by

$$\xi^\alpha = \frac{\partial x^\alpha}{\partial s}, \tag{4}$$

where $s$ is the parameter indexing neighboring geodesics. We can calculate the rate of change of $\xi^\alpha$ with respect to the affine parameter of the geodesic,

$$\frac{d}{d\tau}\xi^\alpha = u^\beta \nabla_\beta \xi^\alpha - \Gamma^\alpha_{\beta\gamma}\xi^\gamma u^\beta \tag{5}$$

$$= \xi^\beta \nabla_\beta u^\alpha - \Gamma^\alpha_{\beta\gamma}\xi^\gamma u^\beta, \tag{6}$$

where we have used the identity [28]

$$u^\beta \nabla_\beta \xi^\alpha = \xi^\beta \nabla_\beta u^\alpha \tag{7}$$

which is valid for geodesic deviation vectors. Writing explicitly

$$\xi^\beta \nabla_\beta u^\alpha = \xi^\beta \frac{\partial u^\alpha}{\partial x^\beta} + \Gamma^\alpha_{\beta\gamma} u^\gamma \xi^\beta \tag{8}$$

yields

$$\frac{d}{d\tau}\xi^\alpha = \xi^\beta \frac{\partial u^\alpha}{\partial x^\beta}. \tag{9}$$

The four-velocity of a blob ejected from a Schwarzschild black hole with negligible angular momentum is

$$u^\alpha = \left(\frac{e}{1-\frac{2M}{r}}, -\sqrt{\frac{2M}{r} - (1-e^2)}, 0, 0\right)^\alpha. \tag{10}$$

For relative motion between particles at the center of the blob and particles at the edge of the blob in the radial direction,

$$\xi^\alpha = (0, R, 0, 0)^\alpha. \tag{11}$$

Plugging Eq. (11) into Eq. (9) gives

$$\frac{1}{R}\frac{dR}{d\lambda} = -\frac{M}{r^2\sqrt{-1+e^2+\frac{2M}{r}}}. \tag{12}$$

Note that substituting $t$ for $\lambda$ in Eq. (12) and then taking a derivative with respect to $t$ with $M/r \to \infty$ reproduces the tidal acceleration of Newtonian gravity: $a_{\rm tidal} \sim MR/r^3$.

Substituting the orbital radius $r$ in place of $\lambda$ in Eq. (12) and integrating, we get

$$\int_{R_0}^{R} \frac{dR'}{R'} = -\int_{r_0}^{r} \frac{M dr'}{r'^2(-1+e^2+\frac{2M}{r'})}, \tag{13}$$

where $R_0 \ll r$ is the initial size of the blob and $r_0$ the starting orbital radius of the blob. Assuming that the blob is ejected from the ISCO radius, $r_0 = 6M$ for $a = 0$, we obtain

$$\frac{R}{R_0} = \left[\frac{(-2+3e^2)r}{6M+3(e^2-1)r}\right]^2. \tag{14}$$

This change in radius is, in principle, observable and can therefore be used to find the mass of the black hole if $e$ is inferred from the COM trajectory. The constant $e$ can be inferred far away from the black hole where it obeys $e = 1/\sqrt{1-v_{\rm COM}^2}$, where $v_{\rm COM}$ is the COM velocity of the blob at $r \gg M$. Figure 4 shows the radial growth factor for blobs with specific energy $e = 1.0001$, 1.001, 1.01, and 10. Because blobs of smaller $e$ spend more time close to the black hole, the tidal effect is larger the closer $e$ is to unity. In

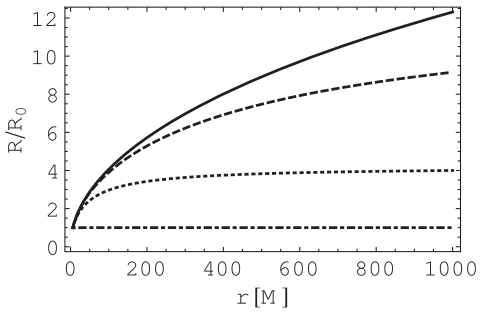


FIG. 4. The growth factor of the blob radius due to gravitational tide as a function of distance from the black hole for a blob moving with negligible angular momentum. The blob's specific energy is $e = 1.0001$, 1.001, 1.01, and 10 for the solid, dashed, dotted, and dot-dashed lines, respectively.

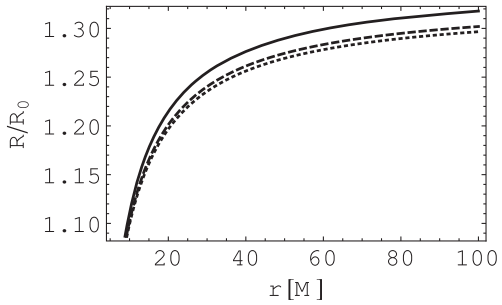


FIG. 5. The growth factor of the blob radius as a function of distance from a spinning black hole for a blob trajectory with a negligible angular momentum. The black hole's spin is $a = 0$, 0.5, and 1 for the solid, dashed, and dotted lines, respectively. The blob energy is $e = 1.2$ for all curves.

the case of $e \sim 1$, one can get a growth factor of $R/R_0 \sim 10$ at $r = 1000M$. This is a change that is observable by the EHT. Assuming that the biggest source of uncertainty is in measuring $R/R_0$, an error propagation calculation implies that the precision of mass measured using this method is $\sim 25\%/\sqrt{N}$, where $N$ is the number of blobs observed. This is competitive with the current measurement precision for M87 [22]. In general, one can also compute the relative motion between the center and the edge of the blob in the $\hat{\phi}$ and $\hat{\theta}$ directions via an analogous calculation.

We can extend this calculation to the case of a spinning black hole with a blob moving radially in the equatorial plane. For this configuration, the relevant components of $u^\alpha$ are

$$u^t = \frac{e}{\Delta}\left(r^2 + a^2 + \frac{2a^2M}{r}\right), \tag{15}$$

$$u^r = \sqrt{e^2 + \frac{2M}{r^3}(ae)^2 + \frac{a^2e^2}{r^2} - \frac{\Delta}{r^2}}. \tag{16}$$

Again we adopt

$$\xi^\alpha = (0, R, 0, 0)^\alpha. \tag{17}$$

Performing an analogous calculation as in the $a = 0$ case, we obtain

$$\frac{R}{R_0} = \frac{R_0\sqrt{a^2(-3+4e^2)M + 36(-2+3e^2)M^3}r^{3/2}}{6M^{3/2}\sqrt{3r^2[2M+(-1+e^2)r] + 3a^2[-r+e^2(2M+r)]}}. \tag{18}$$

If the mass of the black hole and the blob energy $e$ are known, this equation can be used to measure the spin of the black hole. Figure 5 shows the growth factor $R/R_0$ for blobs with dimensionless spin parameters $a = 0$, 0.5, and 1. The effect of spin is weak, and its measurement would be challenging. Again, assuming that the biggest uncertainty is in measuring $R/R_0$, we performed an error propagation calculation to estimate the precision of the dimensionless spin parameter $a$, measured using this technique to be $\sim 0.6/\sqrt{N}$, where $N$ is the number of blobs observed. The current constraint on the spin parameter of M87 is $a > 0.5$ [29].

## V. CONCLUSION

We have shown that observations of ejected plasma blobs from the supermassive black holes Sgr A* and M87 can be used to constrain the spacetime near these black holes. There are two pieces of information that can be obtained from these observations: the blob's trajectory and the tidal effects on the blob's shape.

The trajectory of the blob can be used to limit the presence of nongravitational forces around the black hole or to constrain theories of gravity that predict anomalies in the orbit of test particles in the vicinity of black holes (e.g., Ref. [27]). If a photon ring is detected, its eccentricity could be used as a test of the no-hair theorem. Furthermore, observations of the tidal stretching of the ejected blob can be used to determine both the mass and spin parameter of the black hole.

## ACKNOWLEDGMENTS

This work was supported in part by NSF Grant No. AST-1312034.

[1] M. D. Johnson *et al.*, Astrophys. J. **794**, 150 (2014).
[2] R. Genzel, R. Schödel, T. Ott, A. Eckart, T. Alexander, F. Lacombe, D. Rouan, and B. Aschenbach, Nature (London) **425**, 934 (2003).
[3] I. F. Mirabel, L. F. Rodríguez, B. Cordier, J. Paul, and F. Lebrun, Nature (London) **358**, 215 (1992).
[4] I. F. Mirabel, IAU Symp. **214**, 201 (2002).
[5] I. F. Mirabel, ESA Special Publication **552**, 175 (2004).
[6] A. Babu, arXiv:1407.4258.
[7] N. P. Savani *et al.*, Sol. Phys. **279**, 517 (2012).
[8] E. M. de Gouveia dal Pino and A. Lazarian, Astron. Astrophys. **441**, 845 (2005).
[9] F. Yuan, J. Lin, K. Wu, and L. C. Ho, Mon. Not. R. Astron. Soc. **395**, 2183 (2009).
[10] J. M. Cordes *et al.*, New Astron. Rev. **48**, 1413 (2004).
[11] M. Kramer *et al.*, New Astron. Rev. **48**, 993 (2004).
[12] K. Liu, N. Wex, M. Kramer, J. M. Cordes, and T. J. W. Lazio, Astrophys. J. **747**, 1 (2012).
[13] E. Pfahl and A. Loeb, Astrophys. J. **615**, 253 (2004).
[14] D. Psaltis and T. Johannsen, J. Phys. Conf. Ser. **283**, 012030 (2011).
[15] T. Johannsen, Publ. Astron. Soc. Pac. **124**, 1133 (2012).
[16] R.-S. Lu, A. E. Broderick, F. Baron, J. D. Monnier, V. L. Fish, S. S. Doeleman, and V. Pankratius, Astrophys. J. **788**, 120 (2014).
[17] D. Psaltis *et al.*, arXiv:1411.1454.
[18] S. Bird, W. E. Harris, J. P. Blakeslee, and C. Flynn, Astron. Astrophys. **524**, A71 (2010).
[19] F. Eisenhauer, R. Schödel, R. Genzel, T. Ott, M. Tecza, R. Abuter, A. Eckart, and T. Alexander, Astrophys. J. **597**, L121 (2003).
[20] A. M. Ghez *et al.*, Astrophys. J. **689**, 1044 (2008).
[21] S. Gillessen, F. Eisenhauer, S. Trippe, T. Alexander, R. Genzel, F. Martins, and T. Ott, Astrophys. J. **692**, 1075 (2009).
[22] J. L. Walsh, A. J. Barth, L. C. Ho, and M. Sarzi, Astrophys. J. **770**, 86 (2013).
[23] S. Chandrasekhar, *The Mathematical Theory of Black Holes* (Oxford University Press, Oxford, 1983).
[24] J. Dexter and E. Agol, Astrophys. J. **696**, 1616 (2009).
[25] T. Johannsen and D. Psaltis, Astrophys. J. **718**, 446 (2010).
[26] M. J. Rees, Nature (London) **211**, 468 (1966).
[27] S. B. Giddings, Phys. Rev. D **90**, 124033 (2014).
[28] E. Poisson, *A Relativist's Toolkit* (Cambridge University Press, Cambridge, England, 2004).
[29] S. S. Doeleman *et al.*, Science **338**, 355 (2012).